applied optics

Near-zone transmission caustic of a hanging water drop

James A. Lock

Physics Dept., Cleveland State University, Cleveland, Ohio 44115, USA (retired) (e-mail: j.lock@csuohio.edu)

Received 13 February 2020; revised 3 May 2020; accepted 3 May 2020; posted 4 May 2020 (Doc. ID 390328); published 10 June 2020

A water drop hanging from a house siding board after a rain shower is near-normally illuminated by sunlight either shortly after sunrise or before sunset. A focusing caustic consisting of a bright V-shape or U-shape with a small bright elliptical shape immediately above it is frequently seen on the next lower siding board. In addition, there are two broad regions of illumination immediately above the caustic, fanning out to the upper left and upper right. This complicated pattern, composed of a bright V-shape or U-shape, and the bottom half of the small bright elliptical-shape immediately above it, is caused by the hyperbolic umbilic diffraction caustic near the condition of maximum focus. This can be observed because, by a stroke of good fortune, the distance between the lower edge of a siding board and the flat portion of the next siding board beneath it is nearly equal to the paraxial focal distance of the caustic. Blocking off the light incident on the top, bottom, left side, and right side of the drop was used to determine the portion of the drop responsible for different parts of the caustic. The results were found to match the predictions for the hyperbolic umbilic caustic.

https://doi.org/10.1364/AO.390328

1. INTRODUCTION

After a gentle rain either shortly after sunrise or shortly before sunset, the sun emerges from behind the clouds and illuminates a water drop hanging from the protruding lower edge of a wooden board, aluminum siding, or vinyl siding that covers the exterior vertical surfaces of a house (see Fig. 1). An optical caustic of the light transmitted through the drop appears on the flat portion of the next lower board of house siding. If the water drop is relatively large, the caustic consists of a bright approximately V-shape with opening angle Ψ or a bright U-shape (which could equally correctly be called a V-shape with a very wide opening angle), and a small bright approximately elliptical-shape within the V or U. In addition, two broad swaths of illumination fan out to the upper left and upper right above the caustic. These relatively large hanging drops of different sizes produce a wide variety of opening angles, $80° \leq \Psi \leq 150°$ (see Figs. 2 and 3). On the other hand, if the water drop is relatively small, only the approximate V-shape appears, and the opening angle is in the range $60° \leq \Psi \leq 70°$ (see Fig. 4). This caustic can also be produced with the sun low in the sky by placing a drop of water on the protruding lower edge of a board of house siding using an eye dropper. The water volume of the hanging drop can easily be varied in this way, and one can examine how the details of the caustic depend on the drop size.

The bright approximate V-shape or U-shape and the bright lower perimeter of the approximate elliptical-shape within the V or U together are an example of a hyperbolic umbilic optical caustic near the condition of its maximal focus [1–5]. This caustic is visible, by a stroke of good fortune, because the distance between the outward-projecting bottom edge of a board of house siding and the flat portion of the next lower board (about 10 mm for standard American residential vinyl siding) is nearly equal to the paraxial focal length of the drop. The fine interference structure associated with the caustic [1–5] is not visible for incoherent white light illumination since the size of the caustic on the siding is a few mm, while the details of the interference structure for coherent monochromatic illumination are a few orders of magnitude smaller [6]. The hyperbolic umbilic caustic along with its fine structure have been previously studied in the laboratory using laser illumination and liquid drops with somewhat different shapes. Specifically, Nye studied the transmission caustic of a drop of water clinging to the circular depression cut into a few layers of clear tape placed on a vertical pane of glass and illuminated horizontally by a laser [3,4]. Similarly, Tanner studied the transmission caustic of a drop of oil that was slowly draining down a vertical pane of glass and illuminated horizontally by a laser [7,8]. Marston and his collaborators [6,9–12] (see also [13]) studied the caustic produced by light exiting an acoustically levitated oblate spheroidal water drop after one internal reflection. The geometry here differs from that of Nye and of Tanner in that, in their experiments, the side of the water drop was attached to the glass plate, whereas for the observations reported here, the top of the drop is attached to the house siding.

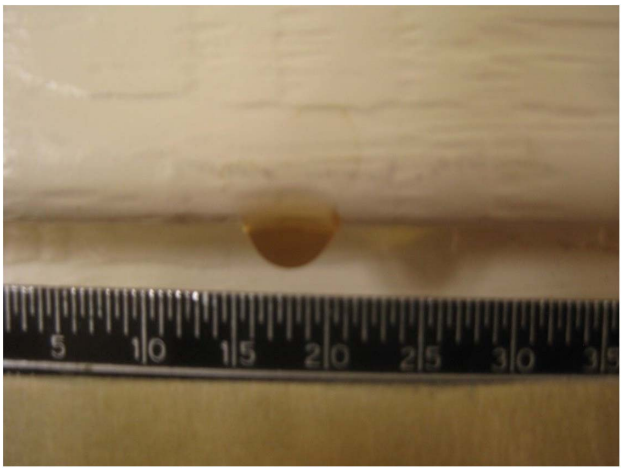

Fig. 1. Water drop (containing brown pigment for clarity) hanging from a board of vinyl house siding. The scale beneath the drop is given in millimeters.

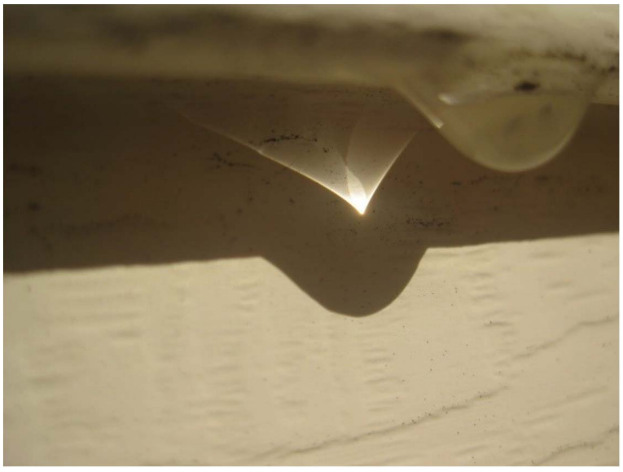

Fig. 2. Near-zone transmission caustic of a large hanging water drop. The opening angle of the caustic near its lowest point is $\Psi = 78^\circ \pm 1^\circ$.

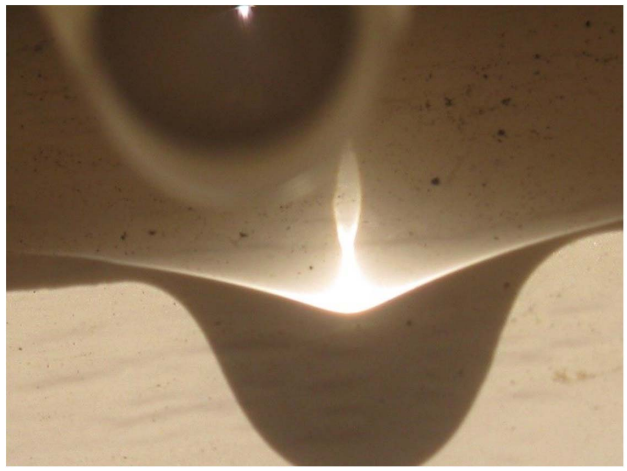

Fig. 3. Near-zone transmission caustic of a very large hanging water drop. The opening angle of the caustic near its lowest point is $\Psi = 141^\circ \pm 1^\circ$.

Fig. 4. Near-zone transmission caustic of a small hanging water drop. The opening angle of the caustic near its lowest point is $\Psi = 59^\circ \pm 1^\circ$.

The body of this study is organized as follows. A model for the shape of the hanging drop is proposed in Section 2. A Fourier optics calculation of the transmitted electric field is then carried out in Section 3 for the model drop shape of Section 2. The overall phase of the transmitted light is Taylor series expanded about its umbilic point [2,4], and is then Fresnel diffracted from the drop's exit plane to the viewing screen. This results in the standard form of the total phase function of the hyperbolic umbilic optical caustic [3–5]. Observations of the near-zone transmission caustic are described in Section 4 and are analyzed in terms of the adjustable parameters describing the shape of the hanging water drop. Conclusions are given in Section 5. Lastly, Appendix A gives a qualitative description of various parts of the observed caustic in terms of interactions of various families of incoming and transmitted rays with the surface of the water drop.

2. SHAPE OF A HANGING WATER DROP

The shape of a hanging water drop is determined by the interplay of gravity and surface tension forces, subject to the constraints imposed by the boundary conditions of the drop's attachment to the surface from which it hangs. Numerical solutions of the nonlinear differential equation for the shape of the drop have been obtained for a variety of axially symmetric drops in [14], and references therein. However, the drop's attachment to the lower edge of the siding board is both highly eccentric and irregular, rather than circular, as was assumed in [14]. Thus, the boundary conditions of the connection of the hanging drop to the protruding lower edge of a house siding board will depend on whether the board is clean or dusty, and whether it is initially dry or damp. Although this variability can be expected to affect the reproducibility of the details of the observed caustic, the structural stability of the hyperbolic umbilic caustic [1,2] ensures that it will occur for a wide variety of hanging drops. As a result, a simple model of the shape of the drop is proposed

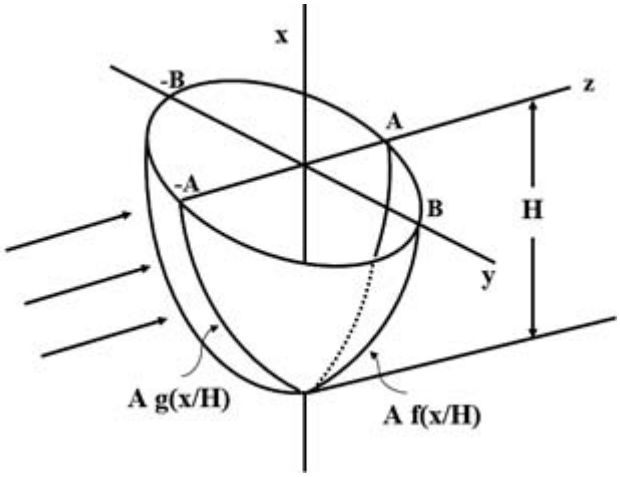

Fig. 5. Geometry of a hanging water drop. The shape profile of the drop is $A\,f(x/H)$ in the x-y plane and $A\,g(x/H)$ in the x-z plane. The incident light propagates in the positive z direction.

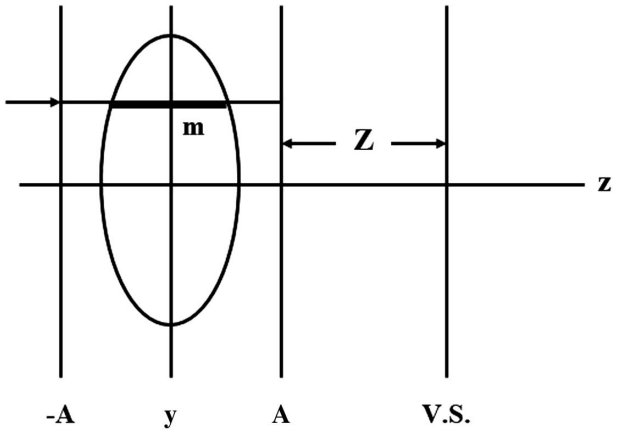

Fig. 6. Ray path through a hanging drop of refractive index m from the $z=-A$ entrance plane to the $z=A$ exit plane. The viewing screen (v.s.) is a distance Z beyond the exit plane.

rather than attempting to numerically solve the governing nonlinear differential equation subject to complicated boundary conditions that are not easily reproducible.

The geometry of the hanging water drop is illustrated in Fig. 5. The positive x direction is vertical, the protruding horizontal lower edge of the siding board is in the $\pm y$ directions, and sunlight is incident in the positive z direction. The length of the hanging drop along the lower edge of the house siding is $2B$ at its attachment, its length there in the direction of the incident sunlight is $2A$, and its height is H. These dimensions are the function of the water volume of the drop. The dimensions of a typical hanging drop of the middle size group, to be discussed in more detail in Section 4, are $2A\sim 3.5$ mm, $2B\sim 5$ mm, and $H\sim 3$ mm. The entrance plane of the water drop is the $z=-A$ plane, and its exit plane is the $z=A$ plane. The viewing screen on which the transmission caustic is observed is a distance Z from the exit plane, as is shown in Fig. 6.

The cross section of the water drop in the $y-z$ plane at the height x with $0\le x\le H$ is modeled here by the ellipse,

$$z^2/a^2+y^2/b^2=1, \tag{1}$$

where

$$a(x/H)=Ag(x/H), \tag{2a}$$

$$b(x/H)=Bf(x/H). \tag{2b}$$

The scaled shape profile of the hanging drop in the x-z plane is $g(x/H)$, and the profile in the x-y plane is $f(x/H)$, where $f(x/H)=g(x/H)=0$ at the bottom of the drop where $x=0$, and $f(x/H)=g(x/H)=1$ at the top of the drop where $x=H$ (see Fig. 5). A one-parameter model of the drop shape uses only a single scaled shape profile, i.e., $g(x/H)=f(x/H)$, and an axisymmetric hanging drop also has $A=B$. As one looks at a hanging drop, one is tempted to describe its shape with the vertical coordinate x being a function of the horizontal coordinate y or z, or ρ in polar coordinates for an axisymmetric drop. But, in Eqs. (2a) and (2b), one takes the vertical coordinate x as the independent variable, and the horizontal coordinate y or z as the dependent variable. The functions $g(x/H)$ and $f(x/H)$ can be expected to have an inflection point where the second derivative of the scaled shape profile with respect to x/H vanishes, i.e., $g''=0$ or $f''=0$. This point marks the transition between the gravity-dominated lower portion of the drop and the boundary-condition-dominated upper portion (see Fig. 10 of [14]). Although g', f', g''', and f''' are all expected to be positive for $0\le x/H\le 1$, g'' and f'' will be negative when x/H is below the respective inflection points, and positive above them.

3. PHASE OF THE ELECTRIC FIELD TRANSMITTED THROUGH THE HANGING DROP

We now show that a wide variety of scaled shape profiles for the hanging water drop will produce a near-zone hyperbolic umbilic transmission caustic. If the hanging water drop was a pure phase object with

$$4\pi A(m-1)/\lambda\ll 1, \tag{3}$$

where m is the refractive index of the drop and λ is the average wavelength of the incident sunlight, an incident ray propagating with the coordinates (x,y) in the positive z direction would travel undeflected through the drop, advancing in phase by $\varphi(x,y)$ from the drop's entrance plane to its exit plane. This assumption underlies Rayleigh–Gans scattering (see pp. 158–165 of [15], and pp. 414–421 of [16] where it is called Rayleigh–Debye scattering). But, for the hanging drops of interest here, $4\pi A(m-1)/\lambda\sim 10^4$ for $m=4/3$ and $\lambda=0.55$ μm. Nonetheless, it is assumed that the electric field transmitted through a hanging drop can be quantitatively analyzed using the methods of Fourier optics (see Section 5.A of [17]), where (i) each ray associated with the incident plane wave advances in phase by $\varphi(x,y)$ as it propagates undeflected through the water drop from its entrance plane to its exit plane, and (ii) the resulting wavefront then propagates via Fresnel diffraction from the exit plane to the viewing screen.

The validity of the Fourier optics approach applied to the hanging drop can be justified as follows. For a plane wave incident on a large oblate spheroid with the aspect ratio $B/A \gg 1$ as in Fig. 5 and approximating a thin lens, the distance from the center of the elliptical cross section of the oblate spheroid to the center of the paraxial focal waist was determined by the author in the course of this study using Fourier optics. The result almost identically agrees with that determined by exact ray tracing. As B/A decreases, Fourier optics overestimate the paraxial focal distance obtained by ray tracing by only ~6% when $B/A = 2$, by ~11% when $B/A = 1.5$, by ~25% for a sphere with $B/A = 1$. In contrast, the comparison quickly becomes quite poor for a prolate spheroid with $B/A < 1$. Since a typical hanging water drop has an aspect ratio of $B/A \sim 1.4$, the features of the hyperbolic umbilic caustic can be expected to be reasonably closely reproduced using the Fourier optics approach.

From Fig. 6, the advance in phase of an incident ray with the coordinates (x, y) from the entrance plane to the exit plane is

$$\varphi(x, y) = 2kA + 2kA\,(m-1)\,g(x/H) \times [1 - (H/B)^2\,(y/H)^2/f^2(x/H)]^{1/2}. \tag{4}$$

We assume the scaled shape profiles $g(x/H)$ and $f(x/H)$ are such that there exists a vertical location x_0 for which

$$(-g_0'')\,f_0^2/g_0 = (H/B)^2, \tag{5}$$

where

$$g_0 \equiv g(x_0/H), \tag{6a}$$

$$f_0 \equiv f(x_0/H), \tag{6b}$$

$$g_0'' \equiv [d^2g/d(x/H)^2]_{x=x0}. \tag{6c}$$

Such a point will in general exist since $g'' < 0$ for x below its inflection point. The point $(x_0, y_0 = 0)$ is called an umbilic point because the wavefront leaving the exit plane in the vicinity of this point is a converging spherical wave [2,4] with small perturbations added, which will partially focus downstream and then diverge. Specifically, the Taylor series expanding Eq. (4) about the umbilic point in powers of the scaled coordinates X and Y, where

$$X = (x - x_0)/H \tag{7a}$$

and

$$Y = y/H \tag{7b}$$

give

$$\varphi(x, y) \approx 2kA + 2kA\,(m-1)\,\{g_0 + g_0'\,X - (1/2)\,(-g_0'') \times (X^2 + Y^2) + (1/6)\,g_0'''X^3 + (1/2)(-g_0'')[2(f_0'/f_0) - (g_0'/g_0)]XY^2 + O(\text{fourth - order terms in } X \text{ and } Y)\}, \tag{8}$$

assuming the coefficients of both X^3 and XY^2 are nonzero. Equation (8) contains only even powers of Y since the shape of the hanging water drop in Fig. 5 is symmetric in y. The converging spherical wave in Eq. (8) is the term proportional to $X^2 + Y^2$, and the perturbations are the terms proportional to X^3 and XY^2. The omitted fourth-order terms in X and Y are assumed to be small as long as X and Y remain relatively small. A hyperbolic umbilic caustic results when both the X^3 and XY^2 perturbations are of the same sign, whereas an elliptic umbilic caustic results when the perturbations are of opposite sign [1–4,18].

The transmitted electric field at the point $(x_{vs},\ y_{vs})$ on the viewing screen a distance Z past the water drop's exit plane is the Fresnel diffraction integral of the phase $\exp[i\varphi(x, y)]$ over the exit plane coordinates (x, y),

$$E(x_{vs},\ y_{vs},\ Z) = \int_{-\infty}^{\infty} dx \int_{-\infty}^{\infty} dy\, E_0 \exp[i\Phi(x, y, x_{vs}, y_{vs}, Z)], \tag{9}$$

where E_0 is the field strength of the incident plane wave and

$$\begin{aligned}\Phi(x, y, x_{vs}, y_{vs}, Z) &= \varphi(x, y) + k(x - x_{vs})^2/2Z + k(y - y_{vs})^2/2Z \\ &= -aX - bY + c(X^2 + Y^2) + \xi X^3 + \eta XY^2 \\ &\quad + O(\text{fourth - order terms in } X \text{ and } Y),\end{aligned} \tag{10}$$

assuming both ξ and η are nonzero. In Eq. (10), one has

$$a = (kH/Z)\,(x_{vs} - x_0) - 2kA\,(m-1)\,g_0', \tag{11a}$$

$$b = (kH/Z)\,y_{vs}, \tag{11b}$$

$$c = (kH^2/2Z) - kA\,(m-1)\,(H/B)^2(g_0/f_0^2), \tag{11c}$$

$$\xi = (kA/3)\,(m-1)\,g_0''', \tag{11d}$$

$$\eta = kA\,(m-1)\,(-g_0'')[2(f_0'/f_0) - (g_0'/g_0)]. \tag{11e}$$

It should be noted that in the one-parameter model of the drop shape with $f(x/H) = g(x/H)$, Eqs. (11c), (11d), (11e) simplify to

$$c = (kH^2/2Z) - kA\,(m-1)\,(H/B)^2\,(1/f_0), \tag{12a}$$

$$\xi = (kA/3)\,(m-1)\,f_0''', \tag{12b}$$

$$\eta = kA\,(m-1)\,(-f_0'')\,f_0'/f_0. \tag{12c}$$

As was shown in [3–5,19], Eq. (10) is recognized as the total phase function of the hyperbolic umbilic optical caustic. Were it not for the perturbation $\xi X^3 + \eta XY^2$, the center of the axisymmetric paraxial focal waist of the converging spherical wave would be located at $a = 0, b = 0$, i.e.,

$$x_{vs} = x_0 + (B^2/H)\,(f_0^2 g_0'/g_0), \tag{13a}$$

$$y_{vs} = 0, \tag{13b}$$

at the viewing screen location $c = 0$, i.e.,

$$Z_{\text{paraxial}} = (f_0^2/g_0)\,\{B^2/[2A(m-1)]\}. \tag{13c}$$

The perturbations $\xi X^3 + \eta X Y^2$ determine the shape of the wavefront aberrations in the focal plane, which is called the focal section of the optical caustic.

Although the interference fine structure associated with the hyperbolic umbilic caustic is obtained by performing the integrations of Eq. (9), the basic structure of the caustic can be obtained using the following catastrophe optics procedure [1,2]. The stationary phase positions of geometrical rays on the viewing screen are given by the vanishing of the gradient of Φ,

$$(\partial\Phi/\partial X) = 0, \tag{14a}$$

$$(\partial\Phi/\partial Y) = 0, \tag{14b}$$

and two or more geometrical rays coincide on the viewing screen when the Hessian second derivative of Φ vanishes,

$$(\partial^2\Phi/\partial X^2)(\partial^2\Phi/\partial Y^2) - (\partial^2\Phi/\partial X\partial Y)^2 = 0. \tag{15}$$

Equation (15) gives the zero-Gaussian-curvature path in the drop's exit plane that will be mapped into the caustic on the viewing screen. Substitution of this path into Eqs. (14a) and (14b) then gives the shape of the caustic.

The approximate solution of Eqs. (14a), (14b), and (15) for the total phase function of Eq. (10) has been discussed in [1–5], and parameter space for the situation studied here is illustrated in Fig. 7. The coordinates on the exit plane of the hanging drop are taken to be (X, Y) relative to the coordinates of the umbilic point. The quantities a and b are taken to be new viewing screen coordinates, since from Eqs. (11a), (11b) the coordinate a is proportional to x_{vs} and b is proportional to y_{vs}. From Eq. (11c), the quantity c is positive when the viewing screen coordinate Z is less than Z_{paraxial}, and c is negative when Z is greater than Z_{paraxial}. The caustic has two disjoint branches when $Z \neq Z_{\text{paraxial}}$. The first is a fold caustic that is approximately parabolic in shape, and the second is approximately a transverse cusp caustic [4,5]. The parabolic fold caustic can qualitatively be thought of as arising from the X, X^2, and X^3 terms of Eq. (10) via the Airy integral {see Eq. (10.4.32) in [20]}. The transverse cusp caustic can be qualitatively thought of as arising from the X, Y, X^2, Y^2, and XY^2 terms of Φ [5]. No light rays are present at any point on the viewing screen below the parabolic fold, two light rays interfere at each point between the fold and the transverse cusp, and four rays interfere at each point inside the transverse cusp.

When $Z = Z_{\text{paraxial}}$, the two disjoint branches of the caustic coalesce into the hyperbolic umbilic focal section (HUFS), a V-shape structure of opening angle Ψ_{HUFS}, where

$$\tan(\Psi_{\text{HUFS}}/2) = [\eta/(3\xi)]^{1/2}. \tag{16}$$

In previous laboratory experiments, when a water drop clings to a depression in a vertical plate of glass with a circular cross section [3], it was found that $\Psi_{\text{HUFS}} \approx 60°$ (see pp. 314–315 of [2] and pp. 496–499 of [21]). Similarly, when an oil drop slowly drains down a vertical glass plate [7,8], again $\Psi_{\text{HUFS}} \approx 60°$. When the HUFS is observed in one-internal-reflection scattering of an acoustically levitated oblate spheroidal drop, $\Psi_{\text{HUFS}} \approx 2\arctan[m/(12^{1/2})]$, where m is the refractive index of the drop [5,19,22]. Lastly, the parabolic fold for $Z < Z_{\text{paraxial}}$ evolves into the transverse cusp for $Z > Z_{\text{paraxial}}$, while the transverse cusp for $Z < Z_{\text{paraxial}}$ evolves into the parabolic fold for $Z > Z_{\text{paraxial}}$ (see Fig. 3e of [1], Fig. 2.5e of [2], and Fig. 4.4 of [4]). When X and Y become sufficiently large in the drop's exit plane, terminating the Taylor series expansion of Φ at third order is inadequate. As a result, the shape of the caustic on the viewing screen for large a and b will be distorted from the localized structure of the hyperbolic umbilic caustic. The distortion is called the global topology of the caustic [1], and is evident in the curvature of the two arms of the V-shape caustic in Fig. 4.

Of particular interest for the observations described here is the relationship between the two branches of the hyperbolic umbilic caustic on the viewing screen and the two disjoint branches of the hyperbola in the exit plane of the hanging drop that are mapped into them. As is illustrated in Fig. 7, the details of the mapping depend on whether $3\xi > \eta$ or $3\xi < \eta$, and whether $c > 0$ or $c < 0$. For the case of $3\xi > \eta$ and $c > 0$ (i.e., $Z < Z_{\text{paraxial}}$), the $X > 0$ branch of the hyperbola in the exit plane labeled by the points 1, 2, 3 in Fig. 7 is mapped into the parabolic fold caustic, also labeled by the same points.

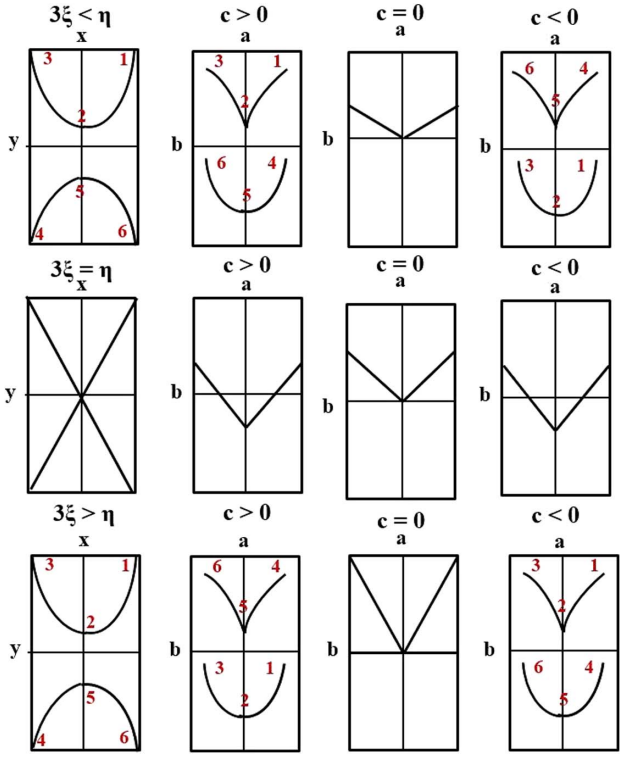

Fig. 7. Locations on the cross section through the hyperbolic umbilic caustic on the $a\,b$ viewing screen (right three columns), corresponding to locations on the hyperbola-shaped zero-curvature path in the $x - y$ exit plane (left column) that is mapped into the caustic, for various values of $3\xi - \eta$ and c of Eqs. (11c)–(11e). The top row corresponds to $3\xi < \eta$, the middle row to $3\xi = \eta$, and the bottom row to $3\xi > \eta$. The opening angle of the $c = 0$ focal section is $\Psi > 90°$ for $3\xi < \eta$, $\Psi = 90°$ for $3\xi = \eta$, and $\Psi < 90°$ for $3\xi > \eta$.

Similarly, the $X < 0$ branch of the hyperbola labeled by the points 4, 5, 6 in Fig. 7 is mapped into the transverse cusp caustic, also labeled by the same points. But, for $3\xi > \eta$ and $c < 0$ (i.e., $Z > Z_{\text{paraxial}}$), the $X > 0$ branch of the hyperbola in the exit plane is mapped into the transverse cusp caustic, and the $X < 0$ branch is mapped into the parabolic fold caustic. When $c = 0$ (i.e., $Z = Z_{\text{paraxial}}$), the two branches of the hyperbola in the exit plane coalesce into two straight lines that cross each other, and one has $\Psi_{\text{HUFS}} < 90°$.

For the case of $3\xi < \eta$, the relation between the two branches of the hyperbola in the exit plane of the hanging drop and the two branches of the caustic observed on the viewing screen is reversed from what it was for $3\xi > \eta$. Namely, the relationship for $c > 0$ is identical to what it was in the former case for $c < 0$, and the relationship for $c < 0$ is identical to what it was in the former case for $c > 0$. For $Z = Z_{\text{paraxial}}$, the opening angle of the HUFS is $\Psi_{\text{HUFS}} > 90°$. Lastly, for $3\xi = \eta$, the observed caustic is the HUFS independent of Z, with the opening angle $\Psi_{\text{HUFS}} = 90°$.

4. OBSERVATIONS OF THE NEAR-ZONE TRANSMISSION CAUSTIC

The transmission caustic of 13 different hanging drops observed on a number of different days was digitally photographed with the solar elevation between 19° and 22° above the horizontal. The opening angle Ψ near the bottom of the caustic was measured to within ±1° in the following way. First, 22 cm × 28 cm printouts of the photographs were made. Then, a pair of straight lines was drawn on the printouts that that visually fit the vicinity of the low point of the V-shape, taking care not to include the region where the sides of the V-shape began to curve. Finally, the angle between the two lines was measured using a 6.3 cm radius protractor.

The transmission caustics and the hanging water drops that give rise to them were subdivided into three groups. The first group of water drops consists of the smallest hanging drops for which a transmission caustic was visible. These caustics consisted of only the approximate V-shape with the measured opening angle being $\Psi = 59°$, 61°, 62°, and 70°, and did not contain the approximate elliptical-shape inside the V (see Fig. 4). They also did not contain the two noncaustic broad swaths of illumination to the upper left and right of the caustic as described in Section 1. The second group of caustics was produced by larger hanging drops where an eye dropper was used to add more water to the hanging drops of the first group. The observed caustics of this group contain the approximate V-shape, the approximate ellipse-shape within the V, and the two broad swaths of illumination to the right and left above the caustic. The bottom of the V and the bottom of the ellipse-shape within it visually appeared to coincide (see Fig. 2). The measured opening angle of the V was $\Psi = 78°$, 86°, 88°, 91°, 98°, and 101°. The third group of caustics was produced by very large hanging drops that were almost ready to drip off the siding board (see Fig. 8). The observed caustics contained an approximate U-shape, rather than a V-shape, and the bottom of the approximate ellipse-shape was noticeably above the bottom of the U (see Fig. 3). The measured opening angle of the U was $\Psi = 135°$, 141°, and 149°. We claim that for the second and third group of caustics, the bright approximate U-shape or V-shape is the parabolic fold branch of the hyperbolic umbilic caustic, and the bright lower half of the perimeter of the approximate ellipse-shape within the U or V is the transverse cusp branch.

Fig. 8. Small hanging water drop and a very large hanging drop, and their near-zone transmission caustics. The values of A and of B at the attachment of the drops to the house siding are nearly equal for both drop sizes.

A. Transmission Caustic of the Small Drops of the First Group

We first consider the smallest hanging drops that produce only the V-shape caustic with $59° \le \Psi \le 70°$. As a starting approximation for $f(x/H)$ in the one-parameter model, the solution of Eq. (6) of [14] for the shape of an axially symmetric drop very near to its low point is a hyperbolic cosine, which when converted to the normalization of Section 2 gives

$$f(x/H) = \text{arccosh}[(x/H) + 1]/\text{arccosh}\,(2). \tag{17}$$

For this approximation to the drop shape, the opening angle Ψ_{HUFS} is found to weakly depend on B/H. For example, when $B/H = 0.833$ one obtains $x_0 = 0.205$, $f_0 = 0.478$, and $\Psi_{\text{HUFS}} = 59.71°$, while for $B/H = 0.625$ one obtains $x_0 = 0.1143$, $f_0 = 0.360$, and $\Psi_{\text{HUFS}} = 59.90°$.

Alternatively, one could consider the normalized version of the first term in the Taylor series expansion of Eq. (17),

$$f(x/H) = (x/H)^{1/2}, \tag{18}$$

which corresponds to a drop whose shape is a paraboloid. For this example,

$$x_0 = (1/4)\,(B/H)^{1/2}, \tag{19}$$

$$f_0 = (1/2)(B/H), \tag{20}$$

$$\xi = \eta = 4kA(m-1)/(B/H)^5, \tag{21}$$

$$\Psi_{\text{HUFS}} = 60°, \tag{22}$$

independent of B/H. If the shape of the hanging water drop was instead a half-ellipsoid,

$$f(x/H) = [2(x/H) - (x/H)^2]^{1/2}, \tag{23}$$

the first term of its Taylor series expansion would match that of Eqs. (17) and (18), and the coefficient of the second term would differ only slightly from that of Eq. (17). For this example,

$$x_0 = 1 - [1 - (B/H)^2]^{1/2}, \tag{24}$$

$$f_0 = B/H, \tag{25}$$

$$\xi = \eta = kA\,(m-1)\,[1 - (B/H)^2]^{1/2}/(B/H)^5, \tag{26}$$

and again

$$\Psi_{\mathrm{HUFS}} = 60^\circ, \tag{27}$$

independent of B/H. The HUFS opening angles of Eqs. (17), (18), and (23) are equal, or nearly equal, to the value found in the experiments of Nye [3,4] and of Tanner [7,8], where the drop was supported in a very different way. It is also in general agreement with the observations of the caustic of the first group of hanging water drops as in Fig. 4 if one assumes that the viewing screen is at the HUFS, or very close to it.

This claim was tested as follows. Since the hyperbolic umbilic caustic is a three-dimensional structure, varying the location of the viewing screen will illuminate different cross sections through the caustic. Thus, one should be able to determine the location of the HUFS as being the location where the two disjoint branches coalesce. Toward this end, a piece of paper was placed on top of the next lower siding board and was then moved inward toward the drop. As this was done, the opening angle of the V-shape narrowed, and a parabolic fold caustic came into view just blow the cusp point. This is consistent with the initial viewing screen position being at the paraxial focus, and the new viewing screen position being at $Z < Z_{\mathrm{paraxial}}$.

In order to view larger viewing screen distances, a different small water drop was suspended using an eye dropper from the bottom free edge of an extra unused piece of house siding that was temporarily mounted horizontally. The transmission caustic was observed on a piece of white cardboard that could be easily moved progressively farther behind the house siding. As the viewing screen was moved to increasingly larger values of Z, the opening angle of the V-shape increased from $\Psi \sim 60^\circ$ toward $\Psi \sim 90^\circ$ as was observed for larger drops in the second group described above. As the viewing screen continued to be moved outward to yet larger Z, the opening angle of the V-shape continued to grow to $\Psi \sim 140^\circ$, typical of the very large drops in the third group. For even larger Z, the two arms of the V-shape became more smoothly rounded, more resembling a U-shape than a V-shape.

When Z of the movable viewing screen was sufficiently larger than Z_{paraxial}, it was observed that the transverse cusp caustic started to retract away from the parabolic fold. This was also observed in the experiments of [9–12]. The reason for this is described in Appendix A. Some of the rays incident near the top of the drop that would have otherwise contributed to the caustic on the viewing screen are now blocked by the connection of the hanging drop to the protruding lower edge of the house siding. This blocking has been termed an aperture effect (see pp. 26, 123, 133 of [4]). In the present situation, when the retracting cusp entered the aperturing region, its continued visibility was prevented, leaving only the parabolic fold due to rays refracted through the upper part of the drop.

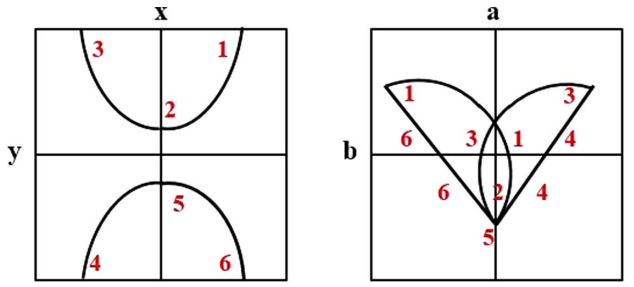

Fig. 9. Locations on the near-zone transmission caustic and the noncaustic features on the ab viewing screen (right) corresponding to rays passing through various locations on the hyperbola-shaped zero-curvature path in the $x - y$ exit plane (left) that is mapped into the caustic.

B. Transmission Caustic of the Larger Drops of the Second Group

In order to determine whether the observed transmission caustic of the larger drops in the second group with $78^\circ \le \Psi \le 101^\circ$ corresponds to $3\xi > \eta$ or $3\xi < \eta$, and to $c > 0$ or $c < 0$, the incident sunlight illuminating different parts of the hanging drop was blocked, and the effect this had on the observed caustic was noted. Even though the blocking was done in the drop's entrance plane, it gives the same result as blocking the same portion of the drop's exit plane, since from ray tracing with $B > A$, paraxial rays incident on the drop to the left and right of center and refracted through the drop do not cross each other until after they have passed the drop's exit plane. It was found that blocking the lower left part of the hanging drop (points 4 to 5 in Fig. 9) extinguished the upper right part of the parabolic fold caustic (again points 4 to 5), and blocking the lower right part of the hanging drop (points 5 to 6 in Fig. 9) extinguished the upper left part of the parabolic fold. Blocking the upper left part of the hanging drop (points 2 to 3 in Fig. 9) extinguished the upper left part of the transverse cusp caustic, and blocking the upper right part of the hanging drop (points 1 to 2 in Fig. 9) extinguished the upper right part of the transverse cusp. These blocking results are consistent with either (i) $3\xi < \eta$ and $c > 0$ (i.e., $Z < Z_{\mathrm{paraxial}}$), giving $\Psi_{\mathrm{HUFS}} > 90^\circ$, or (ii) $3\xi > \eta$ and $c < 0$ (i.e., $Z > Z_{\mathrm{paraxial}}$), giving $\Psi_{\mathrm{HUFS}} < 90^\circ$.

In order to verify that $Z > Z_{\mathrm{paraxial}}$ for the water drops of the second group, a piece of paper was again placed on top of the next lower siding board, and as it was moved inward toward the drop, the V-shape and the elliptical-shape within the V-shape were observed to coincide at the HUFS with $60^\circ \le \Psi_{\mathrm{HUFS}} \le 70^\circ$, and resembled the coma aberration of a thin lens (see Fig. 6.19 of [23]). This test verifies that $3\xi > \eta$, $c < 0$, and $\Psi_{\mathrm{HUFS}} < 90^\circ$ for the caustic of the large hanging drops of the second group.

When describing the blocking experiments, it should also be noted that in the aperturing region where the hyperbolic umbilic caustic is cut off due to the blocking by the lower edge of the house siding, blocking off the top left portion of the hanging drop (point 3 in Fig. 9) extinguished the top left part of the upper portion of the approximate elliptical-shape and the broad swath of illumination to the upper right. Blocking off the top right portion of the hanging drop (point 1 in Fig. 9) extinguished the top right part of the upper portion of the approximate elliptical-shape and the broad swath of illumination to the upper left. This is consistent with the following noncaustic interpretation of these features. Rays with large values of $|y|$ exiting near the top of the hanging drop on the right side are refracted upward and toward the left while other rays exiting near the top on the left side are refracted upward and toward the right. The two sets of noncaustic-producing rays cross each other in the vicinity of the viewing screen. Their overlap on the viewing screen forms the top portion of the approximate elliptical-shape within the V, and the illuminated regions beyond the overlap region are the broad swaths of illumination fanning out to the upper left and upper right above the caustic as mentioned in Section 1.

C. Transmission Caustics of the Largest Drops of the Third Group

As more water is added to a hanging drop in order to advance from drops of the first group, to the second group, to the third group, it was observed that A and B remained roughly constant while H increased (see Fig. 8). From Eq. (13c), Z_{paraxial} is then proportional to f_0 in the one parameter model of the drop shape. Combining this with either Eq. (19) or Eq. (24), one sees that Z_{paraxial} decreases as H increases for constant B. Thus, the next lower house siding board with fixed Z lies progressively farther beyond the paraxial focal distance. This suggests that for the largest drops of the third group $Z \gg Z_{\text{paraxial}}$, and that again the caustic is described by $3\xi > \eta$, $c < 0$, and $\Psi_{\text{HUFS}} < 90°$.

5. CONCLUSION

After a gentle rain, a myriad of water drops hang from various horizontal surfaces, such as twigs of trees, vines, and the horizontal boards of fences. When the hanging drops are near-normally illuminated by the sun low in the sky, light transmitted through them partially focuses as a near-zone hyperbolic umbilic caustic. But, in the usual state of affairs, no viewing screen is located a suitable distance behind the hanging drops, and their transmission caustic goes unnoticed. An exception is provided by the protruding lower surface of a board of house siding, with the viewing screen being the flat surface of the next lower siding board. In this case, the hyperbolic umbilic caustic of the near-zone transmitted light can be easily observed when the sun is low in the sky. The structural stability of this caustic is verified by the wide variety of drop shape profiles $g(x/H)$ and $f(x/H)$ for which the caustic is theoretically predicted to occur. The two branches of the caustic can be understood, either quantitatively using Fourier optics methods augmented by catastrophe optics methods, as in Section 3, or qualitatively by examining the behavior of vertical and horizontal families of geometrical light rays refracted through the hanging drop, as in the following Appendix A.

APPENDIX A

The fact that an incident plane wave transmitted through a hanging drop focuses on a near-zone viewing screen as a hyperbolic umbilic caustic can be qualitatively understood in the following alternative way. Consider first a family of rays propagating in the positive z direction as in Fig. 10, with a constant vertical x coordinate and different horizontal y coordinates. If the hanging drop was a circular cylinder and the horizontal family of rays was transmitted through it, they would form a cylindrical aberration cusp caustic, with three rays passing through any point within the caustic and one ray passing through any point outside. The hanging drop, however, is narrower near its bottom than it is near its top. Crudely modeling it as a tapered cylinder, the apex of the cylindrical aberration cusp will be closer to the drop near the bottom and further from it near the top. If a viewing screen is placed perpendicular to the z axis beyond the cusp apex point for the bottom of the drop, but not as far out as the cusp apex for the top of the drop, the cylindrical aberration caustic will intersect the viewing screen in the shape of a downward-pointing cusp. This is the transverse cusp branch of the hyperbolic umbilic caustic. As the viewing screen is moved further away from the drop, it intersects progressively less of the cylindrical aberration caustic. When the viewing screen is moved past the cusp apex formed by light passing through the top of the drop, the drop's attachment to the lower edge of the siding board completely cuts off the transverse cusp. As was mentioned earlier, this is an example of an aperture effect (see pp. 26, 123, 133 of [4]).

Now consider a family of rays propagating in the positive z direction as in Fig. 11 in the vertical x-z plane. Each ray refracts upward both at its entrance to and its exit from the hanging drop. Thus, one might expect that rays incident near the bottom of the drop would intersect the vertical a axis on the viewing screen lower than rays incident near the top of the drop, due to their lower initial height. But by Snell's law, the lower incident rays refract upward by a greater amount than rays incident near the top of the drop. These two opposing tendencies compete against each other, producing a situation reminiscent of what occurs in the off-axis coma aberration of a thin spherical lens (see Fig. 9G of [24]). Starting with the lowest incident ray and

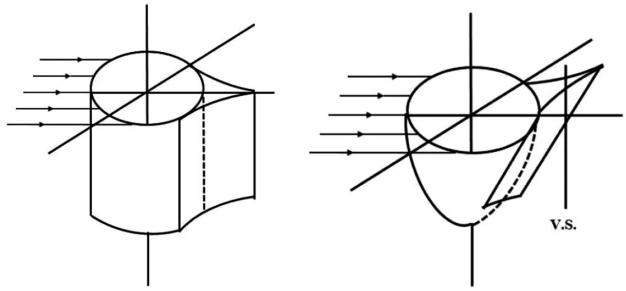

Fig. 10. (a) Cylindrical aberration caustic of a circular cylinder. (b) The cylindrical aberration caustic of a tapered circular cylinder is larger at the top than at the bottom. A viewing screen (v.s.) cuts this aberration caustic in the shape of a downward-pointing cusp.

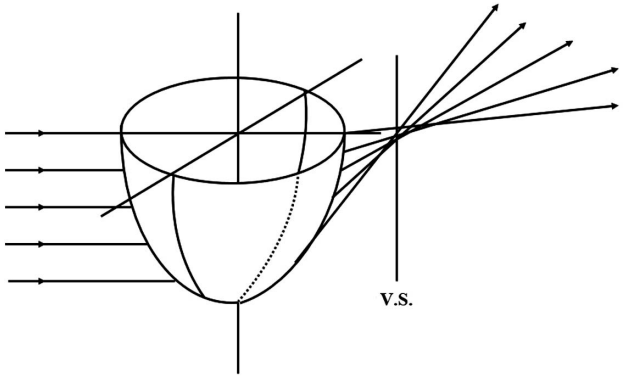

Fig. 11. Light incident on the axis of a tapered cylinder is transmitted through it with a near-zone caustic. A viewing screen (v.s.) cuts this caustic with the contribution of two rays above it and no rays below it.

ending with the highest incident one, the point where a ray crosses the a axis on the viewing screen will first decrease, then reach a relative minimum, and then increase again. This relative minimum position is the low point on the parabolic fold caustic. As is the case for the coma aberration mentioned above, the relative minimum position on the viewing screen is formed by rays leaving the lower portion of the drop when the viewing screen is close to the hanging drop, and it is formed by rays leaving the upper portion of the drop when the viewing screen is far from the drop. The transverse cusp apex and the low point of the parabolic fold subdivide the vertical a axis on the viewing screen into three regions, a zero-ray region below the relative minimum point, a two-ray region between the relative minimum and the transverse cusp apex, and a four-ray region within the cusp. In the two-ray region, each of the contributing rays is a member of the vertical family incident near the middle of the drop. In the four-ray region, two of the rays are members of the vertical families incident near the top and near the bottom of the drop, while the other two are members of a horizontal family that cross each other on the a axis inside the cylindrical aberration caustic.

Disclosures. The author declares no conflicts of interest.

REFERENCES

1. M. V. Berry, "Waves and Thom's theorem," Adv. Phys. **25**, 1–26 (1976).
2. M. V. Berry and C. Upstill, "Catastrophe optics: morphologies of caustics and their diffraction patterns," Prog. Opt. **18**, 257–346 (1980).
3. J. F. Nye, "Optical caustics from liquid drops under gravity: observations of the parabolic and symbolic umbilics," Phil. Trans. R. Soc. London **A292**, 25–44 (1979).
4. J. F. Nye, *Natural Focusing and Fine Structure of Light* (Institute of Physics Publishing, 1999).
5. P. L. Marston, "Geometrical and catastrophe optics methods in scattering," Phys. Acoust. **21**, 1–234 (1992).
6. H. J. Simpson and P. L. Marston, "Scattering of white light from levitated oblate water drops near rainbows and other diffraction catastrophes," Appl. Opt. **30**, 3468–3473 (1991).
7. L. H. Tanner, "A study of the optics and motion of oil droplets," Opt. Laser Technol. **10**, 125–128 (1978).
8. L. H. Tanner, "The form and motion of draining oil drops," J. Phys. D **18**, 1311–1326 (1985).
9. P. L. Marston and E. H. Trinh, "Hyperbolic umbilic diffraction catastrophe and rainbow scattering from spheroidal drops," Nature **312**, 529–531 (1984).
10. P. L. Marston, "Cusp diffraction catastrophe from spheroids: generalized rainbows and inverse scattering," Opt. Lett. **10**, 588–590 (1985).
11. P. L. Marston, "Transverse cusp diffraction catastrophes: some pertinent wave fronts and a Pearcey approximation to the wave field," J. Acous. Soc. Am. **81**, 226–232 (1987).
12. C. E. Dean and P. L. Marston, "Opening rate of the transverse cusp diffraction catastrophe in light scattered by oblate spheroidal drops," Appl. Opt. **30**, 3443–3451 (1991).
13. J. F. Nye, "Rainbow scattering from spheroidal drops—an explanation of the hyperbolic umbilic foci," Nature **312**, 531–532 (1984).
14. J. F. Padday, "The profiles of axially symmetric menisci," Phil. Trans. R. Soc. London **A269**, 265–293 (1971).
15. C. F. Bohren and D. R. Huffman, *Absorption and Scattering of Light by Small Particles* (Wiley, 1983).
16. M. Kerker, *The Scattering of Light and Other Electromagnetic Radiation.* (Academic, 1969).
17. J. W. Goodman, *Introduction to Fourier Optics* (McGraw-Hill, 1968).
18. M. V. Berry, J. F. Nye, and F. J. Wright, "The elliptic umbilic diffraction catastrophe," Phil. Trans. R. Soc. London A **291**, 453–484 (1978).
19. J. A. Lock and F. Xu, "Optical caustics observed in light scattered by an oblate spheroid," Appl. Opt. **49**, 1288–1304 (2010).
20. M. Abramowitz and I. A. Stegun, *Handbook of Mathematical Functions* (National Bureau of Standards, 1964).
21. M. V. Berry, "Singularities in waves and rays," in *Physics of Defects, Les Houches Session XXXV-1980* R. Balian, M. Kléman, and J.-P. Poirier, eds., (North Holland, 1981), pp. 453–543.
22. P. L. Marston, C. E. Dean, and H. J. Simpson, "Light scattering from spheroidal drops: exploring optical catastrophes and generalized rainbows," in *AIP Conference Proceedings* (American Institute of Physics, 1989). Vol. **197**, pp. 275–285.
23. E. Hecht, *Optics*, 2nd ed. (Addison-Wesley, 1987).
24. F. A. Jenkins and H. E. White, *Fundamentals of Optics* (McGraw-Hill, 1950).